On easterly changes over elevated terrain in Australia's southeast

Graham A. Mills

Bureau of Meteorology Research Centre, Australia, and
Bushfire Cooperative Research Centre, Australia

(Manuscript received August 2006; revised April 2007)

This investigation of the structure and evolution of easterly changes through the southern highlands of New South Wales, Australia, was initially prompted by the apparent association of a band of extremely low humidity that was observed just before an easterly change in Canberra on the afternoon of 18 January 2003 (the day of the catastrophic bushfires) with the passage of that cool change. A broader investigation of similar extreme drying events revealed ten easterly change events over the highlands of southeastern Australia that were preceded by similar marked reductions in near-surface humidity. An interesting feature of several of these events is the presence of a long, narrow, dark (dry) band in the water vapour channel (6.7 μ) geostationary satellite imagery parallel to the easterly cool change.

These ten events show a remarkably similar structural evolution, with frontogenesis commencing during the morning near the top of the coastal escarpment, but inland penetration of the cool change not commencing until a deep mixed layer has formed over the plateau on the warm side of the developing front and the frontal temperature gradient has increased to near the maximum value it attains on a given day. It is shown that while these 'easterly cool changes' have gravity-current like characteristics, which has led to them being considered sea-breeze fronts, their origin appears to be on the escarpment rather than the coastline.

A strong, thermally direct cross-frontal circulation is a common feature of these fronts, and the strong pre-frontal ascent generates a gravity wave in the more stable westerly flow above the deep mixed layer on the warm (western) side of the front. It is hypothesised that the narrow, dark (dry) bands seen in the water vapour channel (6.7μ) geostationary satellite imagery mark the downward motion on the eastern (downstream) side of this gravity wave. It is also hypothesised that the strong vertical motions associated with the cross-frontal circulation enhance the entrainment of dry mid-tropospheric air from just above the mixed layer, thus leading to the near-surface humidity reductions observed just before frontal passage.

Introduction

Important components of fire weather forecasting are the timing of wind changes due to the changes in fire behaviour that can occur with an abrupt wind direction change (Cheney et al. 2001), and variations in the low-level humidity due to its effect on fine-fuel moisture content. Mills (2005a) described aspects of the very strong easterly change that reached Canberra (Fig. 1 shows the topography of the area, and locations referred to in the text) on the early evening of 18 January 2003, noting its cold-frontal character (although reversed from the normal west-to-east movement of cool changes in southern Australia), and

Corresponding author address: Dr G. Mills, Bureau of Meteorology Research Centre, GPO Box 1289, Melbourne, Vic. 3001, Australia.
Email: g.mills@bom.gov.au

Fig. 1 Locality diagram with topography from the 0.05° meso-LAPS model run used in Mills (2005a). Contours are plotted at 100, 200, 400, 800 and 1200 m. The C and S mark the positions of Canberra and Scone respectively. The rectangle shows the area of the plots from the mesoscale NWP model in Figs 4, 5 and 10.

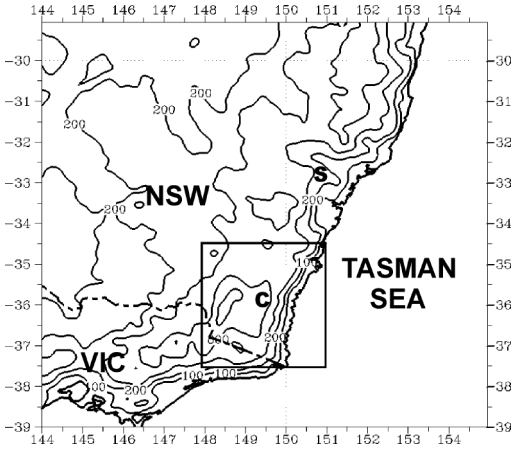

speculated that the extreme near-surface atmospheric drying that occurred just before the cool change was related to vertical circulations associated with the front. In that study, though, a physical link between the drying and the frontal dynamics was not established, although it was postulated that the origin of the dry air at the surface was from a band of dry, mid-tropospheric air seen as a dark band in the 6.7μ Water-Vapour (WV) channel satellite imagery.

The evening easterly change through Canberra is a 'regular' feature of the warm season weather over the Southern Tablelands of New South Wales (NSW) (Taylor et al. 2005). Clarke (1983) documented some aspects of these changes and ascribed them to the inland penetration of a 'sea-breeze-like' circulation that developed on the slopes of the Great Dividing Range. Taylor et al. (2005) ascribed the penetration of these surges to mean sea-level pressure gradient forces between the coast and inland. As part of a broader study into the occurrence and causes of extreme lower-atmospheric drying, prompted partly by the abrupt drying noted in Mills (2005a), it was found that this humidity reduction was a feature common to many of these changes. This paper presents a more detailed examination of the development and evolution of ten such easterly changes over the highlands of southeastern Australia.

The process of case selection used in the study is described first. A particular feature in several of these cases was a long, narrow dark band parallel to the Great Dividing Range seen in WV channel imagery, and because of the association made between WV 'dark bands' and extreme surface drying for the Canberra fire case (Mills 2005a) and for another event over South Australia (Mills 2005b), the relationship between the frontal circulations and these dark lines is one focus of this study. One case, in which a particularly distinct WV imagery dark line was evident, is described in detail. The evolving structure of these fronts is then described, addressing the genesis and evolution of these westward-propagating fronts, the relations between the frontal structure and the dark bands seen in the WV imagery, and the relationship between the frontal circulations and the observed lowering of near-surface humidity just before frontal passage. It will be shown that the features seen in the detailed case study are remarkably consistent from case to case, and the forecasting implications, particularly from a fire weather perspective, will be discussed.

Case selection, data availability, and methodology

The cases that form the basis of this paper were chosen from the larger set selected by algorithms developed to identify 'dramatic drying' cases from the full half-hourly METAR record at a given station. The chief criteria used were that the dew-point should be below –5°C, or below –2.5°C together with a relative humidity less than 10 per cent, subject to constraints based on the variance of the daily dew-point time-series to select only abrupt changes from the background humidity. These latter criteria are used to distinguish abrupt and rapid drying from larger-scale areas of low humidity characteristic of dry continental air masses and are summarised in Mills (2005b). Of the fifteen Canberra cases so selected, the eight cases that preceded evening easterly changes were chosen for closer study in this paper. In addition, two cases when southeasterly changes followed deep drying at Scone (out of the thirteen events there) were included on the basis that linear, coast-parallel dry lines seen in the WV imagery for several of the Canberra cases were also seen in these two cases. Two very clear examples of this linear feature (5 January 2002 and 10 November 2002) are shown in Fig. 2, while the dates of the other events reported in this paper are listed in Table 1.

Fig. 2 **Enhanced (contrast-stretched) water vapour imagery from the GMS-5 geostationary satellite for 0230 UTC 10 November 2002 (top) and 0430 UTC 10 January 2002 (bottom). The arrows indicate the narrow dark band discussed in the text, while 'A' also refers to a feature described in the text.**

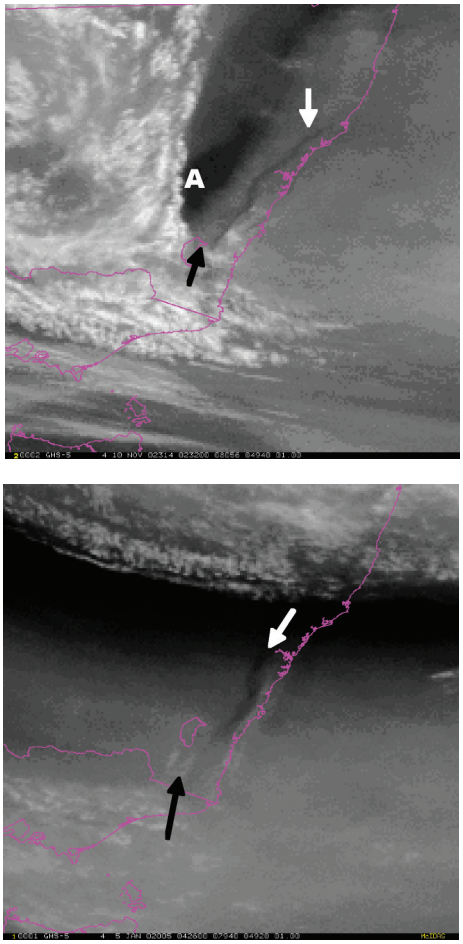

Half-hourly observations from the AWS network operated by the Australian Bureau of Meteorology (the Bureau) were used to select the cases discussed here. The Bureau also operates a hierarchy of internally nested versions of its regional numerical weather prediction (NWP) system; the Limited Area Prediction System (LAPS) (Puri et al. 1998), and the LAPS assimilated analyses were used to describe the synoptic background in which these cool changes occurred. The principal data used in the diagnoses that follow are the archived mesoscale NWP model forecasts from the Bureau's 0.05° latitude-longitude

Table 1. **List of dates at which the easterly change/drying event occurred, the station on which the event selection was based, whether a fine dark band was seen in the WV-imagery for that day (column 3, Yes/No) and the lowest dew-point/relative humidity observed at the station.**

Date YYYY MM DD	*Drying at*	*Fine WV band?*	*Lowest observed dew-point/relh*
2002 01 05	Canberra	YES	- 5.0C/10%
2002 01 12*	Scone	YES	- 3.9C/9%
2002 11 10	Scone	YES	- 5.1C/6%
2003 01 08	Canberra	NO	- 6.2C/12%
2003 01 18	Canberra	NO	-13.0C/4%
2003 01 31	Canberra	YES	- 5.0C/13%
2003 02 12*	Canberra	YES	- 2.8C/10%
2004 02 07	Canberra	YES	- 2.9C/9%
2004 02 29	Canberra	YES	- 6.4C/12%
2005 01 03	Canberra	YES	- 6.1C/9%

grid Sydney region mesoscale configuration (Cope et al. 2004). This particular model was used to access the benefits of hourly model output, together with the highest operational model resolution. Satellite imagery formed an important part of the assessment, particularly to relate the linear features in the WV imagery (e.g. Fig. 2) to the diagnostic interpretation of the NWP model fields.

Diagnosis – case of 10 November 2002

Figure 3 shows the overlaid LAPS analyses of MSLP and of the low-level wind field at 0000 and 0600 UTC 10 November 2002. In Fig. 4 the forecast low-level temperature and wind barbs from the meso-LAPS model based at 1200 UTC 9 November 2002 are plotted at two-hour intervals, and in Fig. 5 the screen-level dew-point forecast from the same model run for mid-afternoon is shown. The broadscale MSLP analyses (Fig. 3) show an anticyclone centred southwest of Victoria with a marked ridge extending along the southern NSW coastline, and strong southerly winds extending northwards with this coastal ridge. The modelled temperature and wind evolution (Fig. 4) shows moderate southwesterly flow over much of inland NSW at the initial time shown (2300 UTC, Fig. 4(a)), with a southerly flow over the Tasman Sea that is tending easterly onshore. The isentropes show a coastal temperature gradient at this time. With time the temperatures rise over the middle of the domain –

Fig. 3 LAPS assimilated MSLP analyses at 0000 (top) and 0600 (bottom) UTC 10 November 2002. The contour interval for MSLP is 2 hPa, and wind barbs at the 0.9943 sigma level are overlayed, with the barbs having their usual meteorological meaning.

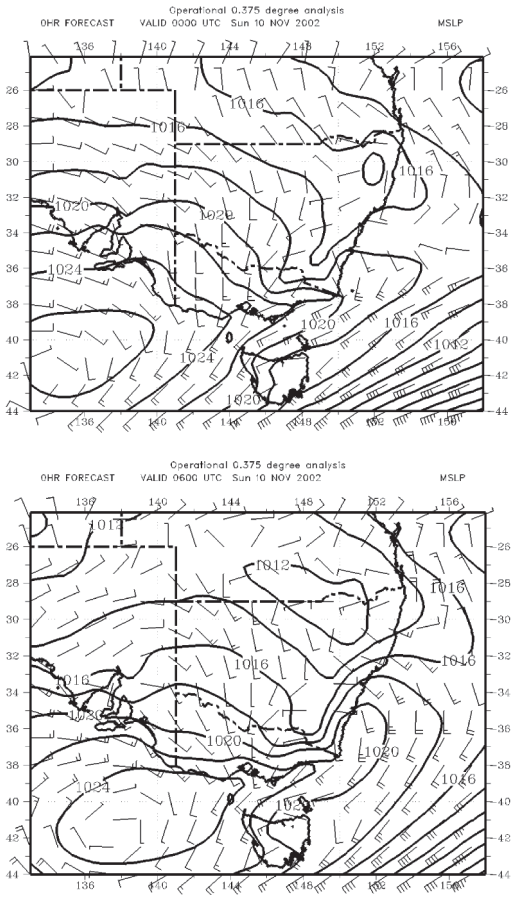

most strongly over the elevated plateau – responding to the diurnal cycle of radiative forcing, but this effect is ameliorated in the western part of the domain by adiabatic cool advection (implicit in the relationship between the wind vectors and the isentropes in Fig. 4). As the onshore winds freshen and back, the cooler maritime air is advected inland, and a front, defined by the convergence of westerly and easterly winds, forms on the eastern slopes of the southern tablelands. The strongest temperature gradient is immediately to the east (cool side) of the wind shift associated with this westward-propagating front. The observed change reached both Scone and Canberra at ~0530 UTC that day, while the meso-LAPS NWP model forecast the change to arrive at ~0700 UTC.

The patterns in Fig. 4 are quite similar to those of the 18 January 2003 event shown in Mills (2005a) (and to those seen in previously published studies of coastal ridging/southerly burster events such as Tory et al. 2001), as is the very strong dew-point front (Fig. 5) that marks the boundary between the dry westerly and the more humid easterly airstream. Again, there is an elongated band of extremely dry air at screen level on the warm side of the front, similar to the 18 January 2003 case. As noted above, a particular feature of this case was the appearance of a long, narrow dark band in the WV imagery (Fig. 2(a)). As best as can be discerned from the hourly imagery available, this band appears between the coast and the ranges during the morning, and propagates inland during the afternoon.

In order to investigate the possible relationships between vertical circulations associated with the front, the low surface dew-points, and the dry bands seen in the WV imagery (Fig. 2), time sequences of two vertical cross-sections, approximately normal to the front, through the model fields are shown in Figs 6 and 7 (locations of sections shown in Fig. 4(e)). While the topography over the northern section is a little lower than the southern, a very similar evolution with time is seen in each. The first cross-sections shown, at 2100 UTC (Figs 6(a), 7(a)) are valid only a little after sunrise, and the isentropes indicate a stable atmosphere over land, with a little less stability in the cooler air over the ocean. Given that Fig. 4 shows low-level easterly flow onshore, the cross-sections suggest that cool air is dammed against the topography of the Great Dividing Range at this time. Between 2300 and 0100 UTC (Figs 6(b), (c) and 7(b), (c)) a mixed layer develops over the plateau, and on the eastern side of the plateau the isentropes become vertically oriented, marking the front. In concert with this process a thermally direct circulation develops near the top of the slope of the topography, and the ascending branch of this vertical circulation intensifies as the horizontal temperature gradient increases (frontogenesis) and the depth of the thermally mixed boundary layer immediately west of the front increases (Figs 6(d), 7(d)). A response to this strong ascent is the development of an upward bulge of the isentropes above the mixed layer directly above the strongest pre-frontal ascent (see circled areas in Figs 6(e) and 7(e)), due to vertical temperature advection, and the consequent development in the westerly flow above the mixed layer of a gravity wave with a deep descending flow to its east.

This gravity wave is a modelled feature, and as such there is no direct verification of the existence of this particular element. However, there are several observed (Ryan and Wilson (1985), Fig. 1; May et al.

Fig. 4 **Meso-LAPS forecasts valid at two-hour intervals from 2300 UTC 9 November to 0900 UTC 10 November 2002 ((a)-(f)). The contours show potential temperature on the model's lowest sigma surface (approx 10 m above ground), and the wind fields are on sigma level 0.9943 (approx 30 m), and the barbs have their usual meteorological meaning. Wind barbs are thinned to every third grid-point for clarity and the contour interval is 2 K.**

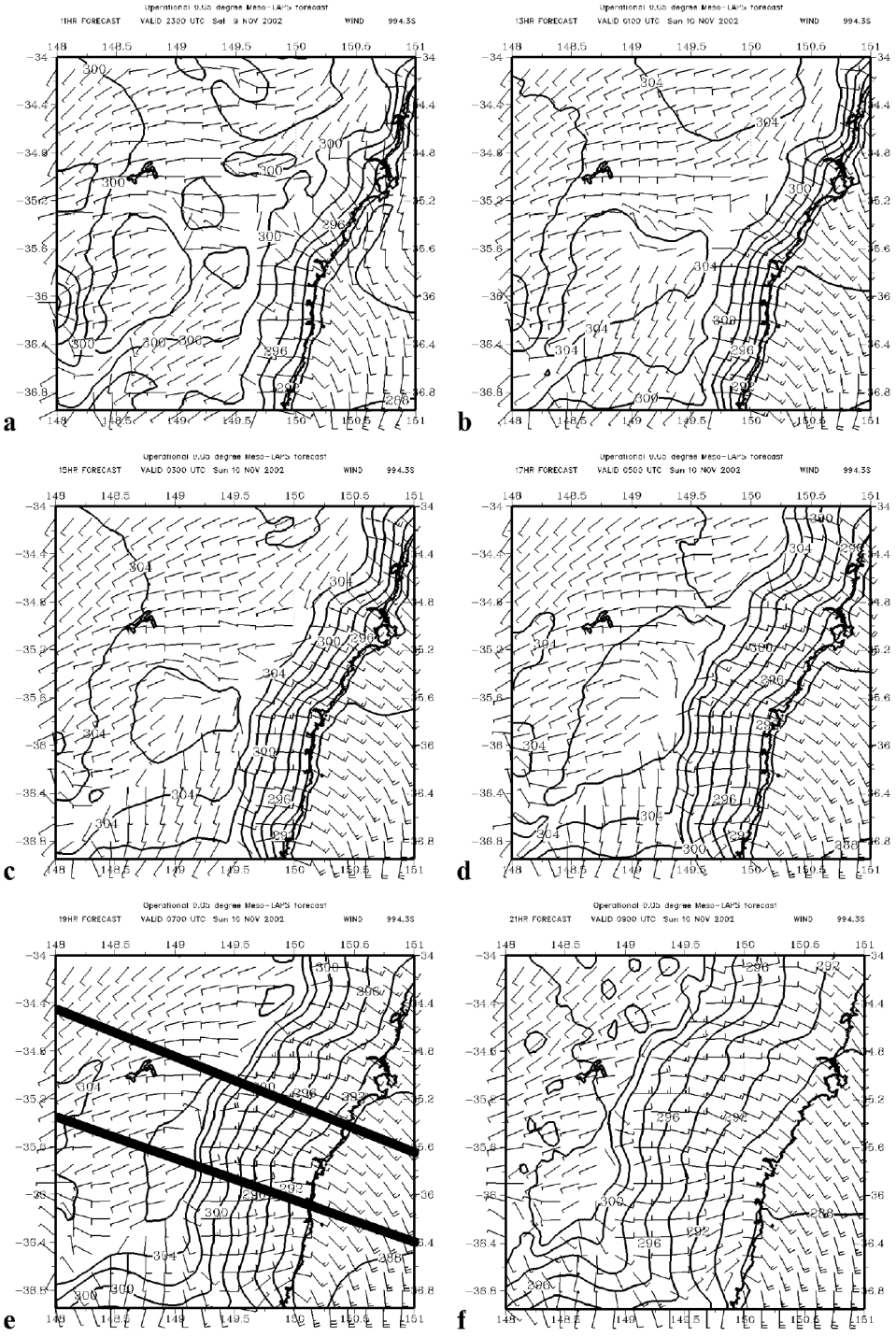

Fig. 5 Meso-LAPS 0.05° forecast of lowest sigma level (approx 10 m) dew-point valid 0700 UTC 10 November 2002. Units are Celsius, with contour interval 1°C.

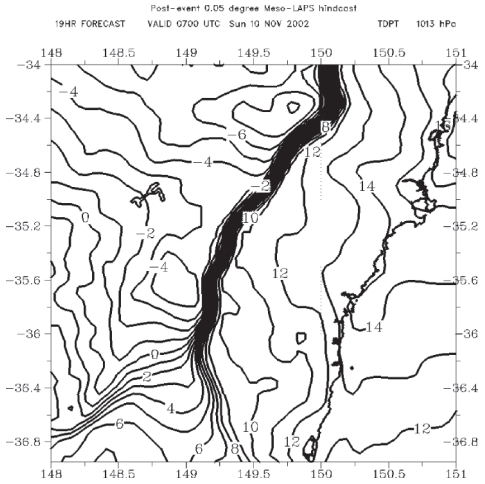

(1990), Fig. 5) and modelled (Keyser and Pecnick (1985), Fig. 5; Reeder (1986), Fig. 5; Garratt and Physick (1986), Fig. 11; Physick (1988), Fig. 3; Garratt et al. (1989), Fig. 6) examples that show a similar feature, and so the feature shown in Figs 6 and 7 cannot be simply dismissed as an artefact of the LAPS model.

With strong daytime heating over the plateau, pressures (geopotential heights) fall there, and, combined with the coastal ridging, this leads to the development of a westward-directed pressure gradient force. In addition, the hydrostatic response to the development of the deep, cool temperature anomaly above the frontal updraft is a local increase in surface pressure below the cool anomaly, and this enhances the developing westward-directed pressure gradient on the warm-air side of the developing front. These processes are summarised in Fig. 8, where the geopotential height profile along the northern section at 925 hPa is shown at three-hourly intervals from 2100 UTC to 0600 UTC. This pressure level was chosen so as to be just above the highest topography along the section, and thus no assumptions as to temperature lapse rates below topography are needed. (This would be necessary if (say) MSLP fields were used to diagnose pressure gradients, yet the resulting pressure gradients are then highly sensitive to the assumed lapse rate.) At 2100 UTC, before solar heating has had significant impact, the height profile is relatively smooth, with an eastward-directed pressure gradient reflecting the larger-scale synoptic pressure pattern. By 0000 UTC heights have risen generally over the whole section, but a small positive perturbation has formed around grid-point 39, together with further rises to the far right (east) of the section as a consequence of the coastal ridging (Fig. 3). There is thus a reversal of the eastward-directed pressure gradient to the west of the local height perturbation near grid-point 39, which is hypothesised to be associated with the developing gravity wave (see Figs 6(c), 7(c)), and also over the coastal waters as a consequence of the coastal ridging. Between 0000 and 0300 UTC geopotential heights fall over the elevated terrain in the middle of the section in response to diurnal heating, leading to a strengthening of the westward-directed pressure gradient just to the east of the plateau, and this effect is enhanced by increasing geopotential heights associated with the coastal ridging. Thereafter heights rise further offshore, and also to the west of the section, but while the minimum height in the section continues to fall between 0300 and 0600 UTC, its location moves westwards. While these processes are not linear in their cause-and-effect, the net result is that after 0300 UTC the front begins to propagate westwards under the influence of this local westward-directed pressure gradient perturbation (Figs 6(e), (f) and 7(e), (f)).

Finally, as the daytime heating decreases and the mixed layer west of the front weakens, the vertical circulations dampen, the isentropes at the frontal 'nose' become more shallowly sloped, and there may even be an acceleration of the front to the west. In this latest stage the speed of movement is perhaps more inferred by the westward movement of the ascent maximum associated with the front, as the position of the maximum temperature gradient becomes more ambiguous with the increasingly shallow slope of the isentropes (Figs 6(g), (h) and 7(g), (h)). Indeed, there is a suggestion that the remnant ascent maximum lies above the developing nocturnal surface inversion east of the plateau in the final panels of Figs 6 and 7.

Gravity wave circulations

It was shown above that the development of a gravity wave above the strongly ascending branch of the frontal circulation leads to the development of significant vertical motion in the westerly flow above the pre-frontal mixed layer. The descent associated with this flow-disruption is strongest in the middle troposphere (600-400 hPa) (Figs 6, 7) between 0500 and 0900 UTC. These are the levels of the atmosphere where the WV channel on the geostationary satellite has its strongest response (Weldon and Holmes 1991). Spatially this descent zone (Fig. 9) also follows the surface front very closely, and so it is most likely that the linear dark feature seen in the WV imagery in Fig. 2 is a result of, and marks the descending part of, the frontally induced gravity wave. In addition, given that this region of descent is

Fig. 6 **(a)-(d) Cross-sections along the northern cross-section line shown in Fig. 4(e). The red (light) contours show potential temperature with a contour interval of 2 K, while the black (dark) contours show vertical velocity with a contour interval of 50 hPa h^{-1} (negative values dashed). The fields are from the 0.05 meso-LAPS model intialised at 1200 UTC 9 November 2002, and are shown at 2 h intervals from 2100 to 0300 UTC. Local daylight savings times (LDST) are shown on the left of each panel.**

Fig. 6 **(e)-(h) Cross-sections along the northern cross-section line shown in Fig. 4(e). The red (light) contours show potential temperature with a contour interval of 2 K, while the black (dark) contours show vertical velocity with a contour interval of 50 hPa hr^{-1} (negative values dashed). The fields are from the 0.05 meso-LAPS model intialised at 1200 UTC 9 November 2002, and are shown at 2 h intervals from 0500 to 1100 UTC. Local daylight savings times (LDST) are shown on the left of each panel. The circle in the top panel highlights the feature discussed in the text.**

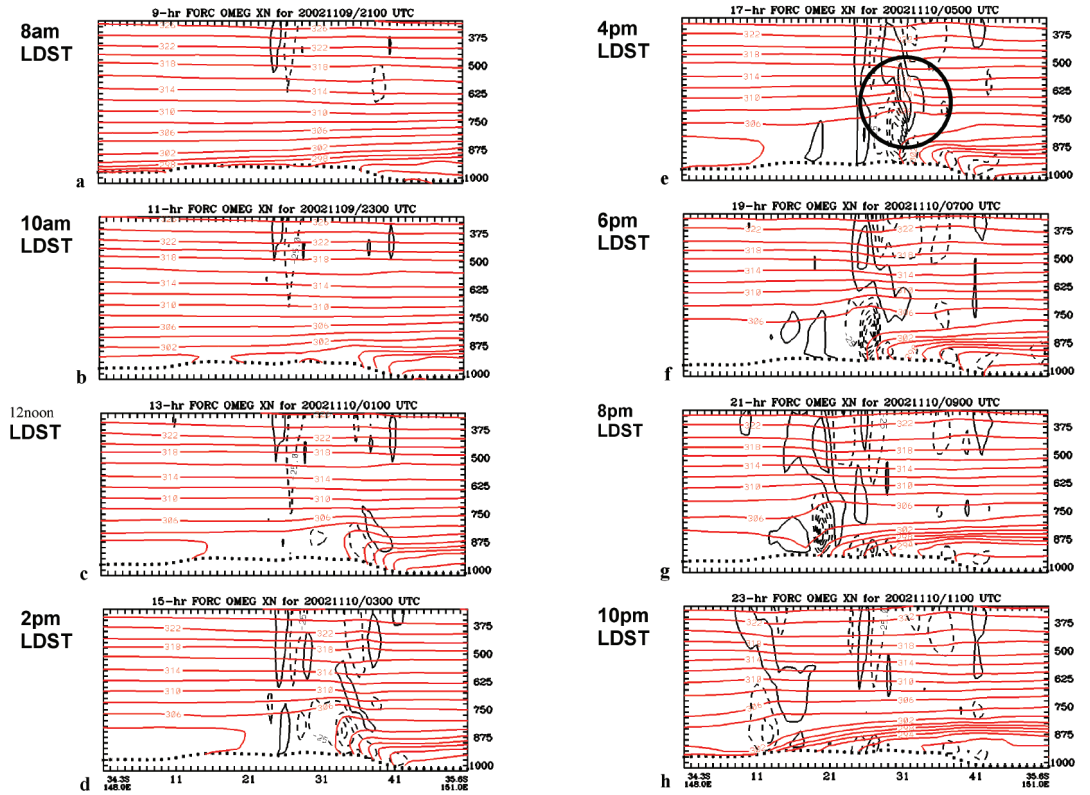

above the cooler and more stable low-level post-frontal flow, it is unlikely that this dark band is a direct indicator of surface drying.

Genesis of the easterly change

The above analysis shows that the easterly change did not propagate from outside the domain, but formed on the slope of the terrain at the boundary between the layer of cool maritime air that had been advected inland and was dammed against the mountains and the hot, dry continental air that overlay this cooler marine layer. Clarke (1983) also noted that his modelled change developed in this location, and suggested that 'in origin it is arguably as much an anabatic wind as a sea-breeze, but it assumes the typical sea-breeze surge structure later in the day'. A recent study by Zawar-Reza and Sturman (2006) shows a very similar easterly change development on the eastern escarpment of the Mackenzie Basin in New Zealand, while Mannouji (1982), Bossert and Cotton (1994),

Fig. 7 **(a)-(d) Cross-sections along the southern cross-section line shown in Fig. 4(e). The red (light) contours show potential temperature with a contour interval of 2 K, while the black (dark) contours show vertical velocity with a contour interval of 50 hPa h^{-1} (negative values dashed). The fields are from the 0.05 meso-LAPS model intialised at 1200 UTC 9 November 2002, and are shown at 2 h intervals from 2100 to 0300 UTC. Local daylight savings times (LDST) are shown on the left of each panel.**

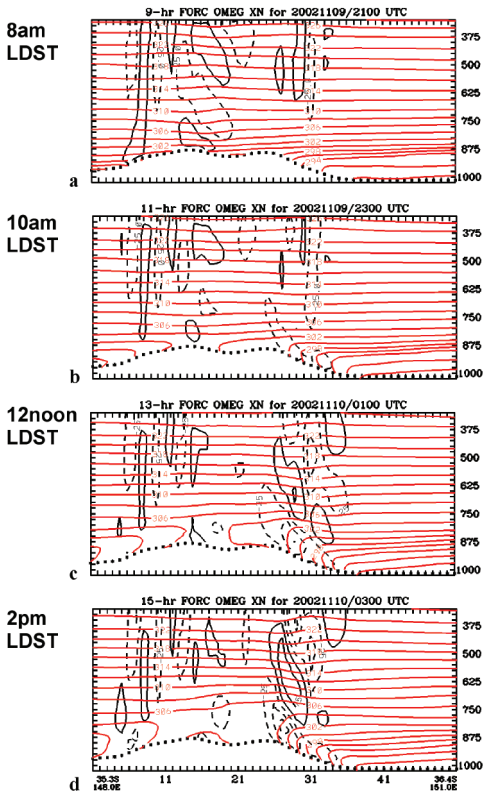

Fig. 7 **(e)-(h) Cross-sections along the southern cross-section line shown in Fig. 4(e). The red (light) contours show potential temperature with a contour interval of 2 K, while the black (dark) contours show vertical velocity with a contour interval of 50 hPa h^{-1} (negative values dashed). The fields are from the 0.05 meso-LAPS model intialised at 1200 UTC 9 November 2002, and are shown at 2 h intervals from 0500 to 1100 UTC. Local daylight savings times (LDST) are shown on the left of each panel. The circle in the top panel highlights the feature discussed in the text.**

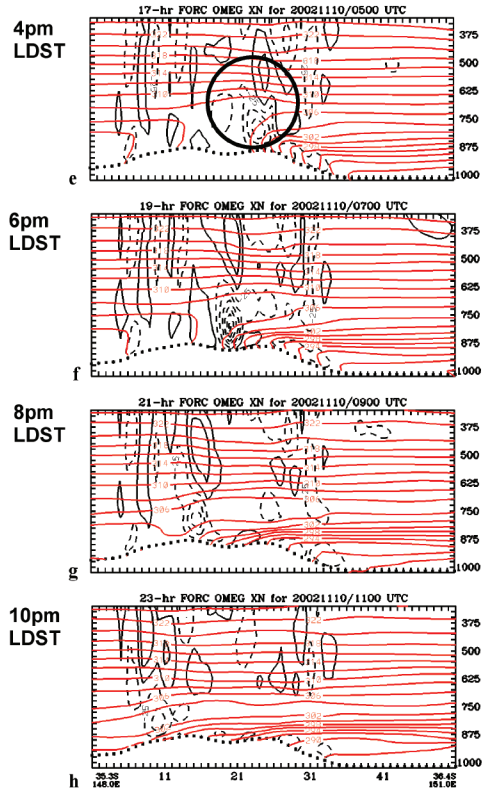

De Wekker et al. (1998), and Doran and Zhong (2000) demonstrate similar plains-to-basin flows in Japan, Colorado, and Mexico respectively.

Parallels could be drawn between what has been shown in this paper and the study of Reeder (1986), with the initial incipient frontal circulation in the present study being due to thermally induced topographic forcing on the background flow, which is enhanced by the cool air associated with coastal ridging being blocked on the eastern side of the topography, rather than Reeder's land-sea contrast thermal forcing. However, in each case the incipient vertical circulation intensifies as the developing front moves into a deep mixed layer (or, perhaps, as a deep mixed layer develops on the warm side of the incipient front). The additional difference of course, is that the change being discussed in this paper moved to the west, rather than to the east.

Relationship between frontal circulations and surface drying

One of the aims of this study was to investigate whether there was a direct or an indirect link between vertical front-induced circulations and the

Fig. 8 **Geopotential height (m) on the 925 hPa surface along the northern cross-section shown in Fig. 4(e) from the meso-LAPS forecasts based at 1200 UTC 9 November 2002, and valid at 2100 UTC 9 November and 0000, 0300 and 0600 UTC 10 November 2002.**

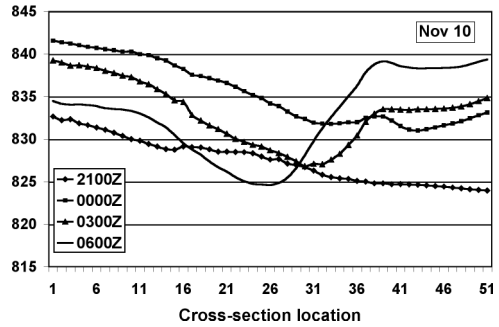

Fig. 9 **Vertical motion on the 450 hPa surface (hPa/h, contour interval 20, negative contours dashed, and zero contour suppressed) from the 18-hour meso-LAPS forecast valid 0600 UTC 10 November 2002. The heavy line shows the 4°C screen-level dew-point contour, which represents the middle of the zone of strongest dew-point gradient marking the westward-propagating front (see Figs 4 and 5).**

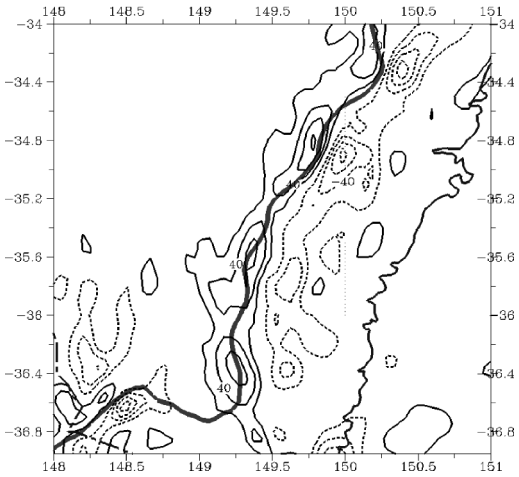

Fig. 10 **Mixing ratio cross-section along the northern section in Fig. 4(e) of modelled mixing ratio valid at 0300 UTC (2 pm LDST). Units of mixing ratio are g Kg^{-1}, with a contour interval of 1.**

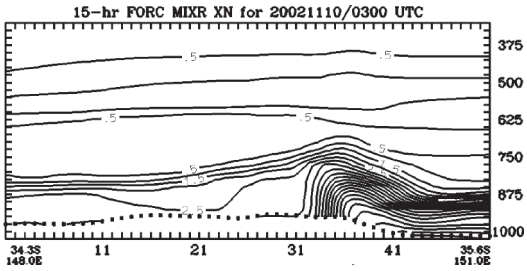

observed surface drying. If a direct link does exist, it would be expected that significant descent would be seen in the warm air (west of surface front). The vertical circulation seen at the front is thermally direct, and so immediately to the warm side of the easterly change there is ascent, although to the west of this ascending stream some descent is seen in the cross-sections, particularly after the front commences its westward movement (see Figs 6(d)-(g) and Figs 7(f),(g)). It is not necessarily clear whether this rate of descent is sufficient to cause the observed drying near the surface by vertical advection alone. The modelled descent rates are ~25-75 hPa h^{-1}; if an air parcel sustained such a descent for some three to four hours then air from around the top of the mixed layer, where very strong moisture gradients are modelled (Fig. 10), could reach the ground. However, in a Lagrangian sense, it is not clear that an air parcel will sustain such a descent rate for the requisite time, and back trajectory analysis would be problematic in a deep mixed layer. Thus the role of this descending branch in the warm air ahead of the front in leading to deep drying is more likely to enhance, or enable, the surface drying process, rather than to be the main driver of such an event. It must be noted that arguments based on the strength of these modelled vertical motions must take account of the strong dependence of their amplitudes on the model configuration (particularly grid-spacing), and that if the modelled descent rates are too weak, then the above conclusion should be revisited.

Entrainment in a convectively mixed boundary layer

Typically, at the top of the convectively mixed boundary layer there is a region of statically stable air where there is entrainment of free atmosphere air downwards, and overshooting thermals penetrating upwards. Stull (1988), p. 473, refers to this as the entrainment zone. As seen in Fig. 10, the air above the mixed layer is much drier than that in the mixed layer,

and therefore entrainment of this air would lead to drying of the air in the mixed layer. According to Stull (1988), p. 120, the time-scale for mixing in the convective boundary layer is of the order

$$t = a\,H/w^* \qquad \ldots 1$$

where a is a constant of O(1), H is the height of the inversion (top of the mixed layer) and w^* is the convective velocity scale. Estimating H as ~3000 m in the middle of the sections in Figs 6 and 7, and w^* as ~1-2 m s^{-1} (Stull 1998), the timescale is ~1500 sec. Thus conservatively, within a timescale of an hour (3600 sec) full mixing of entrained air from the inversion (entrainment) layer at the top of the mixed layer will have occurred. Therefore, if it is to be assumed that abrupt changes in near-surface humidity are due to mixing, then there would need to be either an abrupt change in the humidity of the entrained air or a marked increase in the rate of entrainment. The first situation might occur if a band of drier air moves over the area, as proposed by Mills (2005a) for the 18 January 2003 case (and this might be enhanced by the drier air having a lower virtual potential temperature, leading to a weakening of the inversion/deepening of the convective boundary layer). In the second case, it is a reasonable hypothesis that the strong ascent just ahead of the front would enhance turbulence on the entrainment layer, leading to dry air mixing to the surface via this enhanced entrainment, and also deepen the mixed layer (see the circled regions in Figs 6 and 7). This links the updraft just ahead of the front with the surface drying that appears to be associated with the front, as seen in both this 10 November 2002 case (Fig. 5) and in Mills (2005a), and so might be seen as a plausible working hypothesis.

This hypothesis does not link the narrow dark (dry) band seen in the WV imagery (Fig. 2) directly to the surface drying, but does provide a link between the dry area 'A' in Fig. 2 and the surface drying seen at Scone on 10 November 2002, and is also consistent with the Canberra case described in Mills (2005a). However, given that the strong gravity-wave descent that is hypothesised to cause this dry band is linked to the strong ascent in the mixed layer on the warm side of the front and to frontal movement, the presence of this band may well be an indicator that active frontogenesis and an active vertical frontal circulation are moving westward into a deep mixed layer, provided of course that the humidity structure of the atmosphere is such that the WV imagery can resolve the effects of these vertical circulations.

Other cases

The other cases listed in Table 1 were examined in the same manner as was the November 10 case described in the previous section. The results of this assessment are synthesised in Figs 11 and 12. Figures 11(a) and (b) show, for eight cases, the time sequence of the greatest ascent rate in the cross-frontal circulation, the greatest descent rate in the descending part of the mid-tropospheric gravity wave, and the greatest horizontal (pressure surface) temperature gradient in the lowest 100 hPa of the same cross-section locations discussed in the previous section†. For both sections and for all eight cases the evolution is surprisingly similar, with a rapid increase in maximum temperature gradient and ascent rate until early/mid afternoon, followed by a decrease in the magnitude of these quantities, and a similar evolution for the maximum descent rate in the mid-troposphere. There is some suggestion that the ascent maximum lags (in time) the temperature gradient maximum, and that the descent maximum lags the ascent maximum, but there is some case-to-case variation. These plots do suggest, though, that the intensifying horizontal temperature gradient (frontogenesis) near the top of the topographic slope leads to an intensifying updraft on the warm side of the front. With the decreasing static stability west of the developing front during the daytime heating cycle the amplitude of this vertical circulation increases, consistent with the diagnostic Sawyer-Eliassen equation (Bluestein 1986, pp. 188-92). The vertical advection associated with this ascending branch of the cross-frontal circulation causes the upward bulge in the isentropes above the mixed layer, and the westerly flow at these levels then is forced to ascend on the western (upstream) and then descend on the eastern (downstream) side of this gravity wave.

Figure 12 shows the number of occasions that the maximum temperature gradient was located at a particular cross-section grid-point (see tick marks on the abscissae of Figs 6 and 7) at two-hour intervals. While there is some scatter, it is quite clear that the position of the maximum gradient remains relatively stationary, and very close to the same location near the top of the escarpment in each case, until around 0200 UTC (by which time the majority of the intensification of the thermal gradient and vertical circulation has occurred). After this time the westward movement of the front commences. This is remarkably consistent between the cases. Only at the end of the times shown, when the nocturnal inversion is beginning to form, does the rate of movement begin to show much variability, with a

† These were estimated by eye from printouts of the data generated for the contoured cross-sections such as those in Figs 5 and 6. A horizontal 1:2:1 filter was applied before the assessment.

Fig. 11(a) Time series of greatest ascent, greatest descent, and maximum low-level horizontal temperature gradient along the northern cross-section for the eight cases.

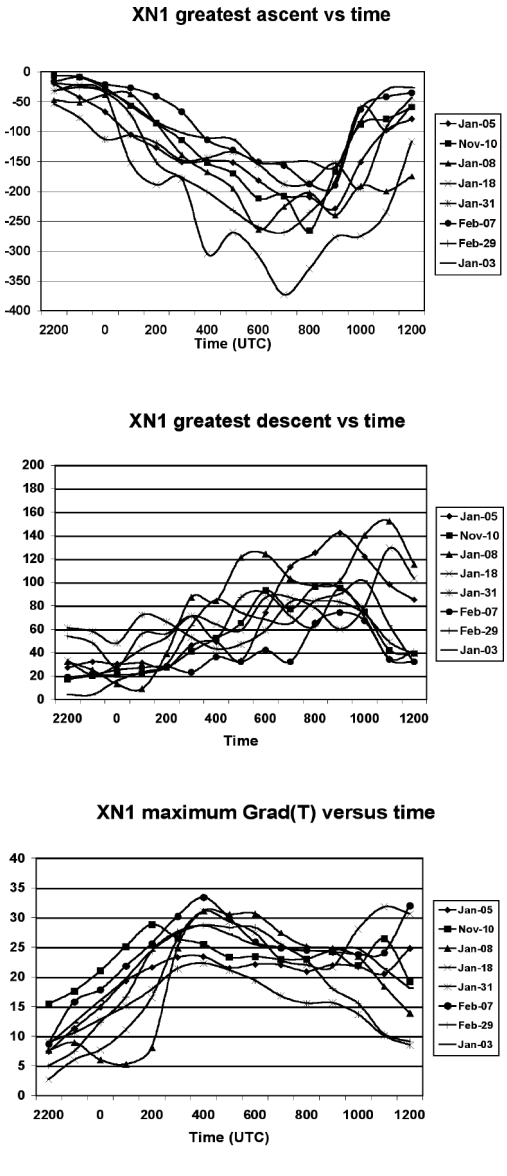

Fig. 11(b) Time series of greatest ascent, greatest descent, and maximum low-level horizontal temperature gradient along the southern cross-section for the eight cases.

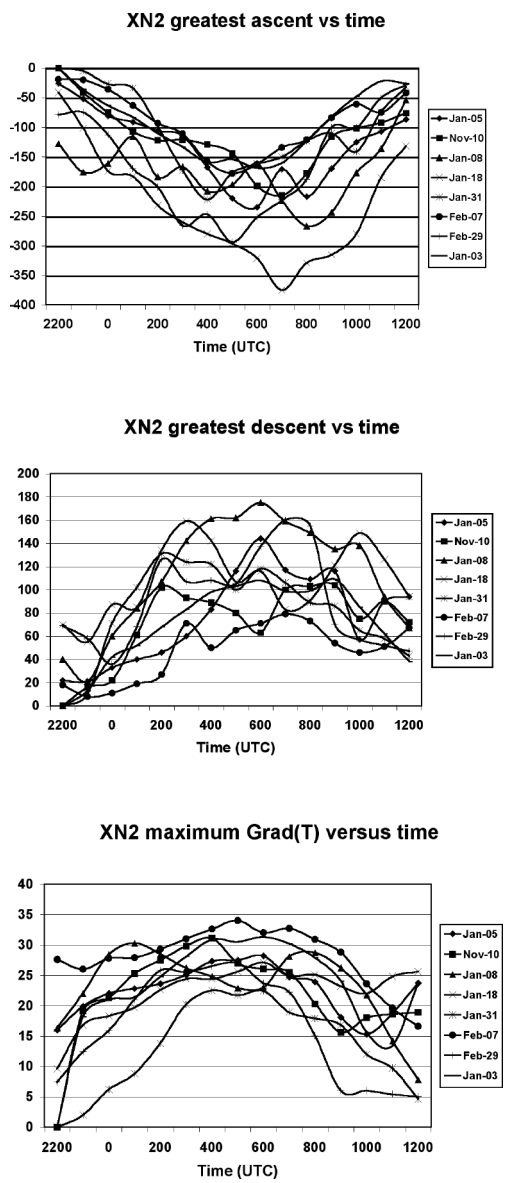

wider scatter of locations in the bottom panels of Fig. 12. Part of the reason for this is the greater ambiguity in the position of the maximum temperature gradient as the slope of the isentropes becomes less steep with the onset of nocturnal cooling. The conclusion is that, at the very least for a significant number of evening easterly changes over the elevated parts of southeastern NSW, the genesis region for the changes is near the top of the topographic slope, not the coastline, and that inland movement commences around 0200 UTC. Thus detection of such changes for nowcasting purposes using an AWS network should take account of this, and not expect a steady inland progression of a sea-breeze circulation from the coast.

Fig. 12 **Position of the maximum low-level temperature gradient along the northern (left) and southern (right) cross-sections, for the model fields at two-hour intervals from 2200 to 1200 UTC for the eight cases. The ordinate is scaled with an interval of 1, while the horizontal tick marks are those of the cross-sections in Figs 6 and 7.**

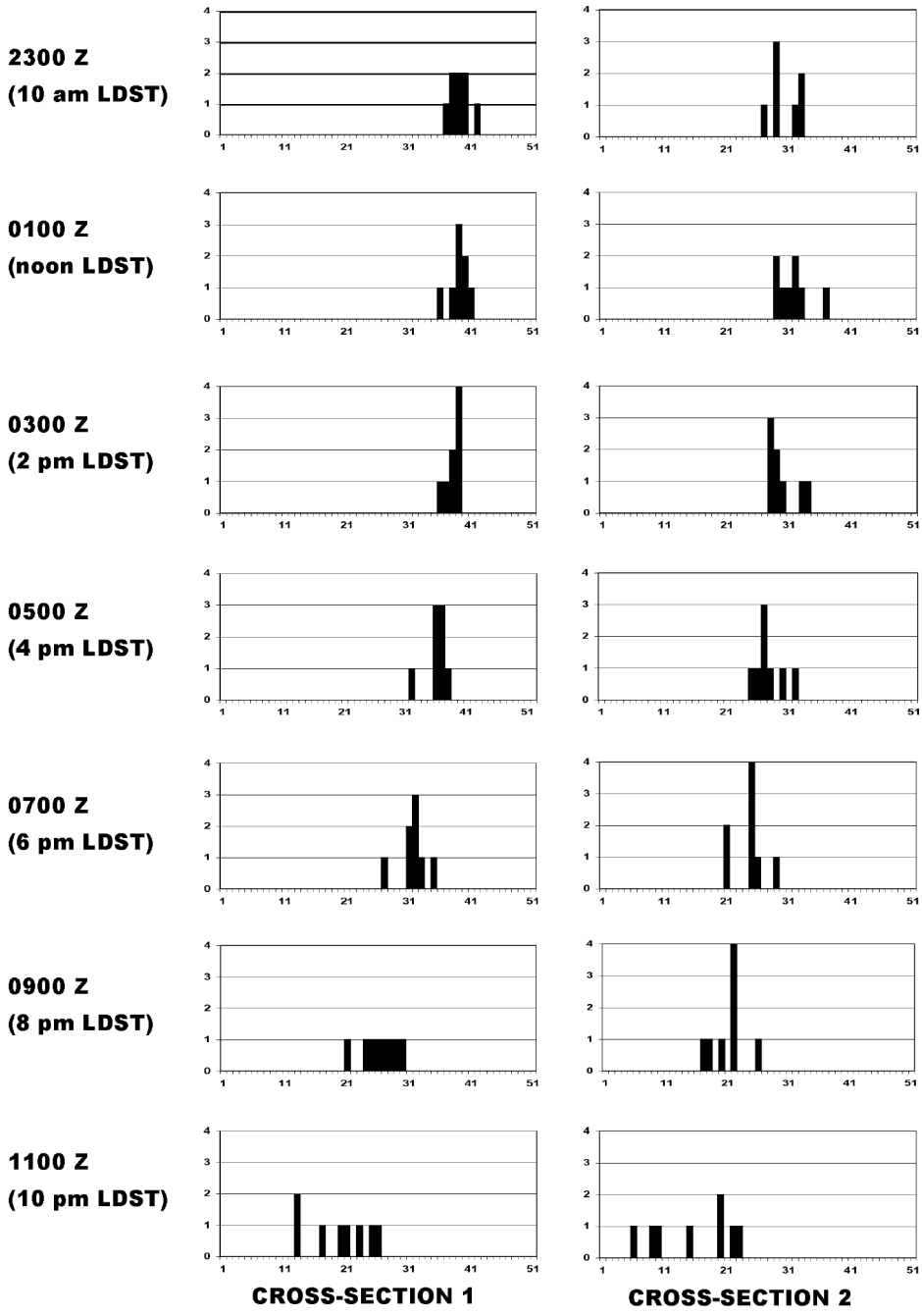

There are of course caveats on the generality of this conceptual model: the cases above were selected by their outcomes – significant and unusual humidity reductions prior to the arrival of an easterly change – and so might perhaps be expected to show some common features. Two of the cases selected (* in Table 1) were not used in the discussion above as the model behaviour was less simple than the other eight, although it must be stressed that even in these cases the pattern of increasing horizontal temperature gradient near the top of the topographic slope, and increasing ascent on the warm side of the thermal gradient during the heating phase of the diurnal temperature cycle was followed. During the first of these cases (12 February 2003) the onshore flow was from the northeast, and the modelled developing change remained largely stationary. The synoptic situation on this day suggested relatively weak dynamics, and so it might be speculated that the rather subtle balance of forces necessary for this change to progress westwards was not well represented in the model's initial state. For the second of these cases (12 January 2002), the model fields show a deeper southwesterly flow approaching the southeast tablelands across the Victorian Alps than was seen in the cases used for Figs 11 and 12. In this case the synoptic forcing was rather stronger, with an active low pressure centre in the Tasman Sea, and the depth of the cold air behind the front was sufficient to preclude the blocking effect of the eastern Victorian ranges that appears to be a necessary condition before coastal ridging along the NSW coast can occur (Lee 2005; Tory et al. 2001).

Discussion

The genesis, structure, and evolution of ten easterly cool change events over the highlands of southeastern Australia have been described in this paper. The analysis reveals a number of interesting features of these westward-propagating fronts. First, the genesis area is near the top of the topographic slope, with a layer of cool air on the eastward (maritime) side of the ranges. The frontogenesis (intensification of the horizontal temperature gradient) occurs as the increasing depth of the cool maritime air and the leftward-turning of the southerly flow associated with the coastal ridge lead to ascent and cool advection on the eastward slopes of the Great Dividing Range (see the temperature/wind relationships in Fig. 4), while diabatic heating over the plateau leads to increasing temperatures and lower surface pressures to the west of the developing front. These two processes lead to frontogenesis near the top of the topographic slope during the early part of the diurnal heating cycle. Thus a common synoptic scenario for these events is one of coastal ridging, a more extreme form of which would be the classic Southerly Burster (Colquhoun et al. 1985). Indeed it is an intriguing question as to whether a necessary prerequisite in order for this frontogenetic process to occur is that the layer of cool air has a depth near to the height of the topographic barrier. While Clarke (1983) noted that his modelled change developed on the topographic slope, he still termed the passage of the change through Canberra as 'sea-breeze like'. This terminology may lead to the expectation that the change will be detectable from near the coast – a better terminology may be to use 'gravity current like' to describe these changes, and thus remove the implication that they have a coastal origin.

Consequences of the frontogenesis are the development of a strong ascending branch of the thermally direct cross-frontal circulation, and the development of a gravity wave structure in the layer above the mixed layer. This gravity wave is revealed as a linear dark feature in WV imagery on those occasions when the background water vapour in the mid-troposphere has suitable characteristics, and was seen on eight of the ten cases examined, although not always as clearly as the examples shown in Fig. 2. The presence of this particular linear dark feature in the WV imagery might well be an indicator of a strong vertical circulation associated with a developing easterly change. It has also been shown that these westward-propagating fronts do not commence their movement until their cross-frontal vertical circulations are well established, and so the presence of the linear dark line in the WV imagery may also be an indication that the change is about to start its westward movement.

A particular feature of the cool change events selected was a dramatic reduction in the near-surface humidity shortly before frontal passage. It is hypothesised that the most likely process leading to the drying is an enhanced entrainment of mid-tropospheric air into the mixed layer due to the very strong ascent associated with the thermally direct cross-frontal ageostrophic circulation.

Acknowledgments

The author has benefited from discussions with Dale Hess and with Michael Reeder during the course of this project, and the reviews of this paper by Kevin Tory, Jeff Kepert and Michael Revell improved the presentation and clarity of the paper.

References

Bluestein, H.B. 1986. Fronts and Jet Streaks: A Theoretical Perspective. *Mesoscale Meteorology and Forecasting*. P.S. Ray, (Ed.) Am. Met. Soc., 793 pp.

Bossert, J.E. and Cotton, W.R. 1994. Regional-scale flows in mountainous terrain. Part II: simplified numerical experiments. *Mon. Weath. Rev., 122*, 1472-89.

Cheney, P., Gould, J. and McCaw, L. 2001. The Dead Man Zone – A neglected area of firefighter safety. *Australian Forestry, 64*, 45-50.

Clarke, R.H. 1983. Fair weather nocturnal inland wind surges and atmospheric bores: Part 1 Nocturnal wind surges. *Aust. Met. Mag., 31*, 133-45.

Colquhoun, J.R., Shepherd, D.J., Coulman, C.E., Smith, R.K. and McInnes, K. 1985. The Southerly Burster of southeastern Australia: an orographically forced cold front. *Mon. Weath. Rev., 113,* 2090-2107.

Cope, M.E., Hess, G.D., Lee, S., Tory, K., Azzi, M., Carras, J., Lilley, W., Manins, P.C., Nelson, P., Ng, L., Puri, K., Wong, N., Walsh, S. and Young, M. 2004. The Australian Air Quality Forecasting System. Part I: Project Description and Early Outcomes. *Jnl appl. Met., 43*, 649–62.

De Wekker, S.F.J., Zhong, S., Fast, J.D. and Whiteman, C.D. 1998. A numerical study of the thermally driven plain-to-basin wind over idealized basin topographies. *Jnl appl. Met., 37*, 606-62.

Doran, J.C. and Zhong, S. 2000. Thermally-driven gap winds into the Mexico City Basin. *Jnl appl. Met., 39*, 1330-1340.

Garratt, J.R. and Physick, W.L. 1986. Numerical study of atmospheric gravity currents. I: simulations and observations of cold fronts. *Beitr. Phys. Atmos., 59*, 282-300.

Garratt, J.R., Howells, P.A.C. and Kowalczyk, E. 1989. The behaviour of dry cold fronts travelling along a coastline. *Mon. Weath. Rev., 117*, 1208-20.

Keyser, D. and Pecnick, M.J. 1985. A two-dimensional primitive equation model of frontogenesis forced by confluence and horizontal shear. *J. Atmos. Sci., 42*, 1259-82.

Lee, J.T. 2005. Effects of Coastal Topography on the Structure and Evolution of Fronts in southeastern Australia. MSc Thesis, School of Mathematical Sciences, Monash University, Australia. 112 pp.

Mannouji, N. 1982. A numerical experiment on the mountain and valley winds. *J. Met. Soc. Japan, 60*, 1085-1105.

May, P.T., Wilson, K.J. and Ryan, B.F. 1990. VHF radar studies of cold fronts traversing southern Australia. *Beitr. Phys. Atmos., 63*, 257-69.

Mills, G.A. 2005a. On the subsynoptic meteorology of two extreme fire weather days during the eastern Australian fires of January 2003. *Aust. Met. Mag., 54,* 265-90.

Mills, G.A. 2005b. Lower atmospheric drying, stability, and increased wildfire activity. *Proceedings, Sixth Symposium on Fire and Forest Meteorology*, Canmore, Canada, October 2005. American Meteorological Society.

Physick, W.L. 1988. Mesoscale modelling of a cold front and its interaction with a diurnally heated land mass. *J. Atmos. Sci., 45*, 3169-87.

Puri, K., Dietachmayer, G.D., Mills, G.A., Davidson, N.E., Bowen, R.A. and Logan, L.W. 1998. The new BMRC Limited Area Prediction System. LAPS. *Aust. Met. Mag., 47*, 203-23.

Reeder, M.J. 1986. The interaction of a surface cold front with a prefrontal thermodynamically well-mixed boundary layer. *Aust. Met. Mag., 34,* 137-48.

Ryan, B.F. and Wilson, K.J. 1985: The Australian summertime cool change. Part III: subsynoptic and mesoscale model. *Mon. Weath. Rev., 113*, 224–40.

Stull, R.B. 1988. *An Introduction to Boundary Layer Meteorology*. Kluwer Academic Publishers. 666 pp.

Taylor, J.R., Kossmann, M., Low, D.L. and Zawar-Reza, P. 2005. Summertime easterly surges in southeastern Australia: a case study of thermally forced flow. *Aust. Met. Mag., 54*, 213-24.

Tory, K.J., Reason, C.J.C. and Jackson, P.L. 2001. A numerical study of a southeast Australian coastal ridging event. *Mon. Weath. Rev., 129*, 437-52.

Weldon, R.B. and Holmes, S.J. 1991. Water vapour imagery. Interpretation and applications to weather analysis and forecasting. *NOAA Technical Report NESDIS, 57*, 213 pp.

Zawar-Reza, P. and Sturman, A.P. 2006. Two-dimensional numerical analysis of a thermally generated mesoscale wind system observed in the Mackenzie Basin, New Zealand. *Aust. Met. Mag., 55,* 19-34.